A High-Performance Ultrafast Humidity Sensor Based on Micro-Knot Resonator-Assisted Mach-Zehnder for Monitoring Human Breath

Yating Yi,[†] Yuxuan Jiang,[†] Haiyan Zhao,[†] Gilberto Brambilla,[‡] Yaxian Fan [§] and Pengfei Wang*,[†,ǂ]

[†]Key Laboratory of In-fiber Integrated Optics of the Ministry of Education, College of Science, Harbin Engineering University, Harbin 150001, China

[‡]Optoelectronics Research Centre, University of Southampton, Southampton SO17 1BJ, UK

[§] Academy of Marine Information Technology, Guilin University of Electronic Technology, Beihai, 536000, China

[ǂ]Key Laboratory of Optoelectronic Devices and Systems of Ministry of Education and Guangdong Province, College of Optoelectronic Engineering, Shenzhen University, Shenzhen, 518060, China

Keywords*: Ultrafast response; humidity sensor; micro-knot resonator; human breath monitoring; fiber-optic device*

ABSTRACT: Monitoring dynamic humidity requires sensors with fast response and anti-electromagnetic interference, especially for human respiration. Here, an ultrafast fiber-optic breath sensor based on the humidity-sensitive characteristics of gelatin film is proposed and experimentally demonstrated. The sensor consists of a micro-knot resonator superimposed on a Mach-Zehnder (MZ) interferometer produced by a tapered single-mode fiber, which has an ultrafast response (84 ms) and recovery time (29 ms) and a large dynamic transmission range. The humidity in a dynamic ambient cause changes in the refractive index of gelatin-coating, which could trigger spectral intensity transients that can be explicitly distinguished between the two states. The sensing principle is analysed using the traditional transfer matrix analysis method. The influence of coating thickness on the sensor's trigger threshold is further investigated. Experiments on monitoring breath patterns indicate that the proposed breath sensor has high repeatability, reliability and validity, which enables many other potential applications such as food processing, health monitoring and other biomedical applications.

Fiber-optical sensors have attracted considerable interest for their unique advantages such as corrosion-free, miniaturisation, light weight and anti-electromagnetic interference. A variety of optic fiber sensors have been reported for measuring temperature,[1-3] humidity,[4-6] refractive index[7-9] and physical and chemical properties.[10-13] Among them, optical fiber humidity sensors are essential for environmental monitoring and are extensively used in food processing, air conditioning, electronic product and medical diagnostics, including human breath monitoring. Human breath has a critical role in non-invasive diagnosis of diseases, both in hospital and at home.[14] Breath frequency and depth could be used to assess human health, and a humidity sensor with continuous monitoring and fast response and recovery time is inevitably required for this task. Mogera et al. reported fast response and recovery speeds (8 and 24 ms, respectively) for a supramolecular nano-fiber-based electronic humidity sensor.[15] Nonetheless, electronic sensors are unsuitable to operate in electromagnetic fields such as those present in a magnetic resonance imaging system. Burman et al. demonstrated the realisation of molybdenum disulphide/graphene oxide (MoS_2/GO) nanocomposite as humidity-sensitive materials for a chemo-resistive humidity sensor.[16] Jha et al. introduced a resistive humidity sensor using tungsten disulphide (WS_2) nanosheets deposited on a silicon/silicon dioxide (Si/SiO_2) substrate containing interdigitated aluminium electrodes, which exhibited a response, changing by ~3.15 times for humidity levels between 40% and 80% relative humidity (RH).[17] Humidity sensors integrated with photonic circuits usually demand expensive and complex preparation; thus, sensors using optic fibers offer a viable route to safer and wider applications for medicine, due to their flexibility, compactness, and immunity to electromagnetic fields and corrosion.

To overcome the limitations of silica-based optical fibers and enhance the sensitivity to RH, a variety of humidity-sensitive media have been extensively discussed as coating layers such as agarose,[18] gelatin,[19, 20] polyvinyl alcohol overlay (PVA),[21, 22] carbon nanotubes[23] and metal oxides.[24, 25] The basic mechanisms of humidity-sensing rely on the variation of the surrounding refractive index (RI) caused by humidity.

In our work, a high-performing, all-optical sensor for humidity measurement based on a micro-knot resonator, incorporating an MZ interferometer, was proposed. A gelatin

film was deposited on the surface of the MZ arm through natural evaporation. The infiltration of ascending water molecules on the gelatin film decreased the RI of the gelatin. The variation of output spectrum and transmission intensity reflected the alteration of the surrounding humidity, allowing the detection of human breath. Within a certain humidity range, the dynamic range of transmission intensity can reach about 25 dB. The corresponding response and recovery speed of the optimised sample were 84 ms and 29 ms, respectively. The influence of the coating thickness on the rise/fall threshold of this optical sensor was also discussed. The experimental results illustrate that the proposed sensor has an excellent sensing performance and can be used for a promising real-time respiratory monitoring application.

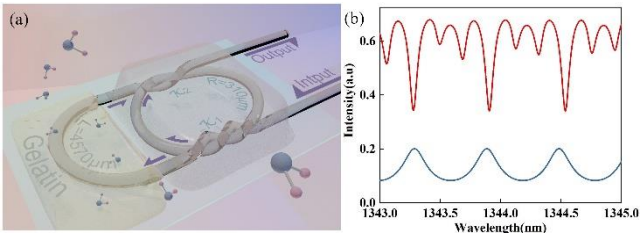

Fig. 1 (a) Schematic configuration and (b) The theoretical spectral response of the proposed sensor for coupling coefficient $\kappa_1 = 0.8$ and $\kappa_2 = 0.5$ respectively. The arrows in Fig. 1a represent the propagation of light at high relative humidity.

Fig. 1a depicts the schematic view of the proposed resonator. The input light is divided into two paths (micro-knot and MZ arm) when passing through the first coupling region and then recombining in the second coupling region, resulting in spectral interference at the output port. The traditional analytical solution based on the transfer-matrix analysis is used to analyse the model:[26] when light can pass through the entire structure unimpeded in a relatively higher humidity condition (Fig. 1b, top), the output transmission function can be defined as the ratio between the output and the input fields:

$$T = E_{out}/E_{in} = A/B \tag{1}$$

where

$$A = exp[b(L_1 + L_2 + \pi R_2) + 2b\pi R_1] - exp(b\pi R_1)\sqrt{(1-\kappa_1)(1-\kappa_2)} + exp[b(L_1 + L_2 + \pi R_2)]\sqrt{\kappa_1\kappa_2} \tag{2}$$

$$B = -1 - exp(2b\pi R_1)\sqrt{\kappa_1\kappa_2} + exp[b(L_1 + L_2 + \pi R_2) + b\pi R_1]\sqrt{(1-\kappa_1)(1-\kappa_2)} \tag{3}$$

Here, $b = -\alpha + j\beta$, where α is the transmission loss and β is the propagation constant of the fiber; R_1 and R_2 are the radii of the knot and the MZ loop; L_1 and L_2 indicate the length of straight sections between the curved part of the MZ loop and micro-knot, and κ_1, κ_2 are the coupling coefficients of two intertwisted regions, respectively. Instead, under the condition of relatively low humidity, the gelatin coating introduces additional loss which is large enough to block the transmission of the optical signal in the MZ arm (Fig. 1b, bottom). Thus, the transfer function of output is described by:

$$T = \frac{exp(b\pi R_1)\sqrt{(1-\kappa_1)(1-\kappa_2)}}{1 + exp(2b\pi R_1)\sqrt{\kappa_1\kappa_2}} \tag{4}$$

Importantly, the diameters of the MZ arm and of the micro-knot are maintained equally in both simulations and experiments to provide regular spectra[27] consistent with previous works. The simulation results are displayed in Fig. 1b.

With the aim of fabricating the proposed humidity sensor, a standard single-mode fiber (Corning, SMF-28) was drawn into a micrometre-diameter fiber by using a micro-heater and taper-drawing system. Usually, the micro-knot resonator is fabricated by cutting the tapered fiber, which is bent and twisted to form a knot and coupled to the other section of the tapered fiber with Van Der Waals forces. However, the section of overlapping fibers could result in inevitable extra transmission loss, which may be significant. In this work, the length of tapered fiber was ~16 mm and minimum diameter ~2 μm. One end was fixed onto a precision three-axis platform (Zolix); the other end was bent 180 degrees to make the tapered sections intersect and form a loop. Pushing the movable side of the fiber into the loop then provides the ideal structure comprising a micro-knot-assisted MZ interferometer, as depicted in Fig. 2a. To improve the stability of the resonator, the whole structure was carefully laid on a magnesium fluoride (MgF_2) glass substrate and then fixed using a low-RI ultraviolet, curable adhesive (Luvantix 373 XP) except on the MZ arms. A gelatin solution was prepared and deposited on the MZ arms. Gelatin powders (Ruibio, BoMei Co. Ltd) were mixed and dissolved in deionised water at a ratio of 5% by weight of solution. The mixture was treated by ultra-sonication for five minutes and heated for 30 minutes to obtain a homogeneous solution and avoid agglomeration. The exposed structure was covered with the prepared gelatin solution and then dried. After cooling at ambient temperature for two hours, the water in the solution gradually evaporated and a relatively homogeneous gelatin layer was formed on the surface of the structure for subsequent humidity-sensing experiments.

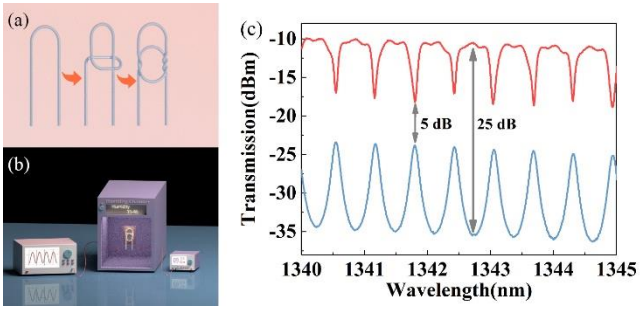

Fig. 2. (a) Schematic of the fabrication process; (b) Experimental setup for measuring the transmission spectrum; (c) Output spectra of two different cases of the resonator.

The light from a broadband emission light source (YSL SC-series) was launched into the input fiber of the fabricated resonator as depicted in Fig. 2b, while the transmission spectrum was monitored using an optical spectrum analyser (OSA) (AQ6317C, Yokogawa, Japan). The output spectrum at ambient temperature in Fig. 2c (blue line) illustrates that the resonator provided a high extinction ratio (ER) (>10 dB) with a small free spectral range (FSR) ≅ 640 pm.

When the ambient humidity increases, the moisture content of the gelatin film increases accordingly. The light passing through the sensing arm will increase with a decrease of

the RI of gelatin coating and interfere with the light passing through the micro-knot in the coupling region, producing an interference pattern that can be very different (red wave in Fig. 2c). The two groups of spectra are symmetrical; a wavelength peak of one corresponds to the resonance dip of the other. As clearly observed from Fig. 2c, the smallest difference in light intensity is the wavelength corresponding to peaks, where the intensity difference is about 5 dB. In the flatter regions between the two peaks, the difference is the largest, reaching 25 dB.

Once the water molecules evaporate from the gelatin coating and the water content descends to the threshold, a transposed condition immediately occurs. This phenomenon can be explained by the dependence of the gelatin RI on its water content. Gelatin is a long, fibrous protein whose RI is higher than that of water.[19] With increasing RH, water molecules diffuse into the gelatin film with holes, and the effective RI of gelatin decreases. Thus, when the relative humidity is low, the gelatin coating with high refractive index will increase light leaking, and only the signal light transmitted through the micro-knot reaches the output port. In contrast, when the humidity in the environment is high enough, the refractive index of the gelatin coating decreases, and the signal light transmitting through the MZ arm interferes with the signal light circulating the micro-knot at the intertwisted area, as indicated by arrows in Fig. 1a.

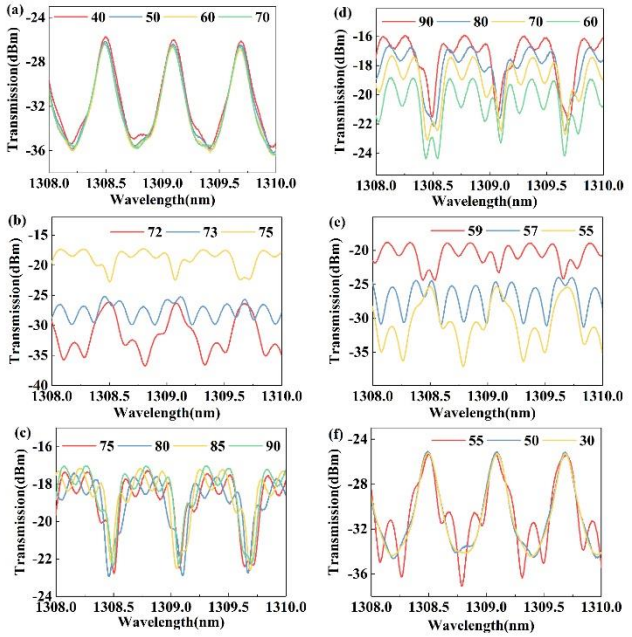

Fig. 3. Variation of spectral transmission at different RH level: (a)-(c) humidity increase process; (d)-(f) humidity decrease process.

To investigate the dependence of the sensor on RH, the resonator was positioned in a controllable environmental chamber (ESPEC SH-222). The resonator was exposed to several complete humidity cycles in the range of 40% to 90% RH in the chamber, with the temperature fixed at a constant value of 37 °C. To enhance the accuracy and stability of the spectrum, each humidity level was maintained for 30 minutes.

The variation of the spectral transmission with RH is presented in Fig. 3. When measured RH changes between 40% and 70% RH with an increment of 10%, the resonance dips experience a slight blue shift with no shape-changes (Fig. 3a). However, once the RH exceeds 72% RH, the profile of the spectrum changes markedly and the transmission intensity grows dramatically with increasing RH, as shown in Fig. 3b. The ripples around 1308.7 nm show a significant red shift when the RH increases from 75% to 90% in 5% step intervals, as shown in Fig. 3c, whereas the shift of dips is irregular, possibly caused by variations of RI and swelling of the gelatin coating at increased water content levels.

It is worth mentioning that when the RH in the environment chamber reaches the threshold value, the spectrum changes in a very short time, showing that it is very sensitive to the humidity change near threshold. The increasing threshold of the resonator should be 73%. When the RH decreases from 90% to 60% in steps of 10%, the transmission intensity decreases regularly, as shown in Fig. 3d. Once the RH declines to 59%, three groups of transmission spectra are recorded at different humidity levels near the threshold. As shown in Fig. 3e, the intensity and the shape of transmission spectra are accompanied by the variation of humidity around the threshold, just as they are opposed to the trend of the spectrum variation when the humidity reaches the humidity threshold in the process of humidity increase. The spectra remain almost unchanged at RH below 55% (Fig. 3f).

Hence, the threshold of the sensor operating at decreasing humidity is ~59%. A reasonable explanation for the different threshold values in the process of increasing and decreasing RH relates to the different distribution of water molecules in the gelatin coating from inside to outside. The coating has a certain thickness, and water molecules need to penetrate into the film and finally reach a stable state; that is to say, when the humidity reaches the threshold and causes spectral changes, the humidity value inside and on the surface of the coating is different. The humidity distribution of the coating decreases from the surface along the radial direction, which means that in the process of increasing RH, if the light intensity increases enough to trigger the spectral change after passing through the MZ arm, the external humidity needs to be higher than the required humidity threshold value inside the coating. If the relative humidity in the environment chamber declines from a high humidity value, the distribution of humidity inside the coating is just the opposite. Water vapour needs to permeate slowly from the inside to the surface until it evaporates into the air, which results in the humidity reduction rate inside the coating becoming much slower than that on the surface of the coating. Thus, we established a simple theoretical model to simulate the variation of transmission intensity caused by the distribution of water molecules inside the film during humidity increase/decrease, and obtained the relationship between relative humidity and light intensity, as shown in Fig. 4c. If the transmitted light intensity of the MZ arm reaches the critical point of triggering spectral changes, a higher humidity environment needs to be provided in the increasing process than in the decreasing process. Based on this, the simulated spectra of the proposed sensor under different RH was obtained, as shown in Fig. 4a, 4b.

To prove the validity of this inference, another reference sample coated with two layers of gelatin was prepared by repeating the depositing process two times. The

corresponding experimental results are displayed in Fig. 4d, with an increased threshold to 95%. Thereafter, when the humidity in the environment chamber was reduced, the shape of the spectrum was observed to change immediately, indicating that the threshold value was reached. Since the humidity in the environment chamber is close to the limit, the film does not continue to absorb more water molecules, and the water content inside the coating is always in the critical state of threshold. This proves that the thickness of gelatin coating is an important factor affecting the threshold.

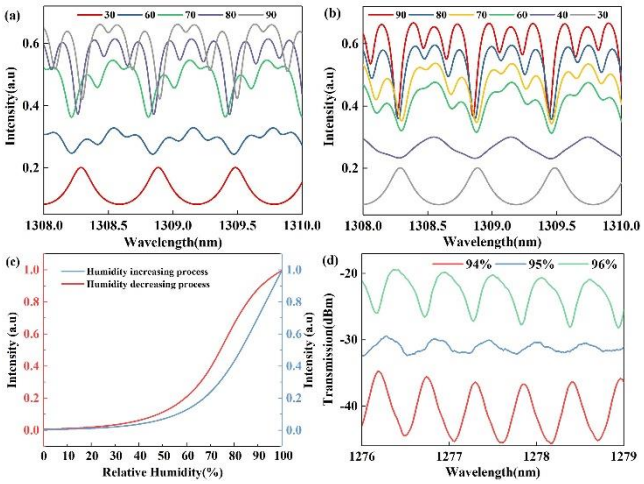

Fig. 4. (a) Simulated spectra during humidity increase; (b) simulated spectra during humidity decrease; (c) simulation of relative humidity and light intensity at the end of the MZ arm; (d) Spectral transmission near threshold of the reference sample.

The response time is a significant indicator for humidity sensors, especially for breathing sensors, when the response speed to environmental humidity changes is particularly important. The light from a Raman fiber laser (Precilasers RFL, 1150 nm, 20 W) was detected by an oscilloscope (Tektronix MDO4034C), after passing through the proposed sensor and a photo-amplifier used to amplify the signal. The resonator was put in the environment chamber with a stable humidity as previously described, and then the chamber cover was suddenly opened to expose the sensor to indoor circumstances to achieve the effect of a sudden drop in humidity. The response times turned out to be 0.63s, 1.23s and 1.74s when the RH declined from 75%, 85%, 95% to the room humidity (see Fig. 5a). The sensor fabricated in this work presented a fairly fast response compared with previous sensors published in the literature. In addition to this, the feature of insensitivity to the temperature of the resonator is shown in Fig. 5b. The humidity threshold measured at different temperatures is stable, as displayed in Fig. 5c.

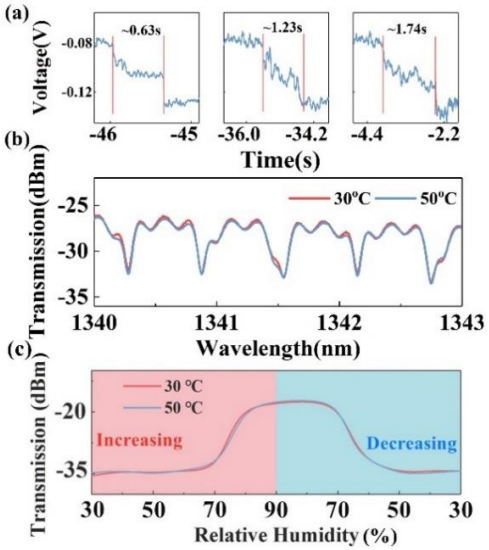

Fig. 5. (a) Response characteristic of the sensor when the RH changed from 75% (left), 85% (middle), 95% (right) to the room humidity of 40% RH; (b) Temperature dependence of the fabricated sensor; (c) Change in the transmitted light intensity during a humidity change period at different temperatures.

The unique transmission spectrum and fast response speed of the proposed resonator makes it attractive for applications in human respiratory monitoring. In the experiment of breath detection, the sensor was fixed on a breathing mask, which was put on volunteer's head to create an ideal detection environment, as illustrated in Fig. 6a.

The detection of nasal breathing can eliminate the interference of mouth saliva. The variations of voltage measured by the oscilloscope could be used to display humidity changes visually in inhalation and exhalation in real time as depicted in Fig. 6b. With the action of exhaling, the voltage immediately rises sharply and then maintains a relatively stable state. Due to the fluctuations of air flow and humidity, the detection results are inevitably disturbed by noise. During inhalation, the detected voltage drops suddenly until it returns to its pre-expiratory state. The recovery time measured during breathing detection is much faster than the response time in the earlier humidity experiments. This is because the air flow velocity is affected by exhalation and inhalation, which changes the humidity in the mask more rapidly and accelerates the evaporation of water molecules inside the coating. Since the thickness of the coating also has an impact on the response time[20] and threshold, a trade-off should be made to select the parameters suitable for the experimental requirements.

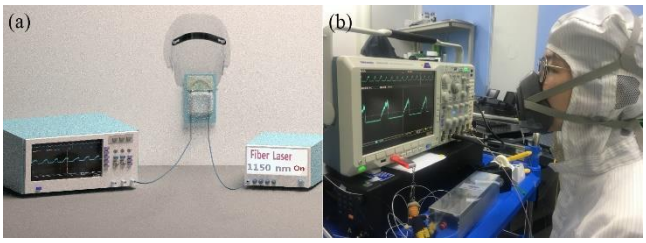

Fig. 6. (a) Experimental setup for the measurement of the breath sensor response time; (b) A photograph of a volunteer performing breathing trials.

With the aim of verifying the response of the resonator to different respiratory frequencies, three groups of rhythmic respiratory frequencies were validated. The results exhibited efficient traces regardless of how fast or slow the volunteer was breathing, as displayed in Fig. 7.

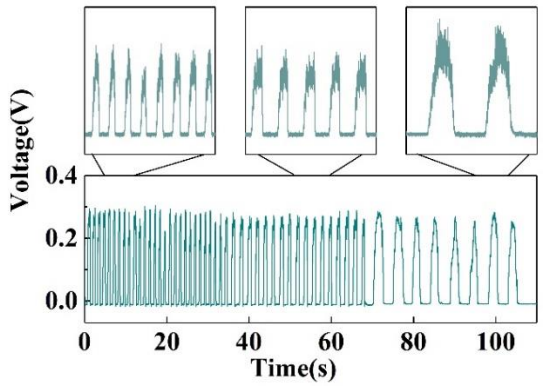

Fig. 7. Response characteristic of the sensor under hybrid breaths. Enlarged views of hybrid breaths are shown above.

Enlarged views in Fig. 7 show the results for 32, 20, and 10 breaths per minute, respectively. They represent three typical respiratory rates from rapid to slow. The corresponding response and recovery times are illustrated in Fig. 8. The analysis of the results shows that the sensor provides excellent tracking on respiration at various frequencies, and the advantages of threshold effect and ultra-fast response are very distinct in the experiment. Even if the humidity changes caused by each breath are different, they satisfy threshold conditions and can be detected without distinction. Besides, the intensity detected is very consistent to actual breaths, as is the logic value commonly used in digital circuits, where only 1 and 0 are used to represent the two states of breathing, which brings inherent superiority to the subsequent data analysis. In contrast, the detection intensity of previous breath sensors in literature is readily affected by other factors such as humidity and airflow, which brings uncertainty to effective detection. Moreover, the sensor maintains very high detection accuracy for several weeks, indicating high repeatability and good long-term stability. The fastest response and recovery times of optimised samples were found to be 84 ms and 29 ms, respectively.

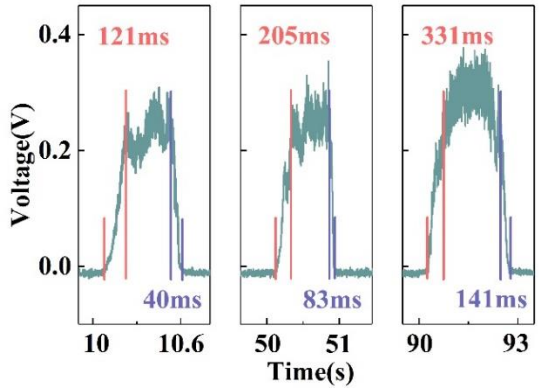

Fig. 8. Response and recovery times of the sensor on different breathing patterns.

Table 1. Comparison of sensing performance obtained by different methods.

Sensor	Response Time/s	Recovery Time/s	Dynamic transmission range/dB
Gelatin-based device (This work)	0.084	0.029	25
WS_2-coated side polished fiber (SPF)[28]	1	5	6
3D graphene network-coated tapered fiber[4]	4	23	35
Reduced graphene oxide (RGO)-coated SPF[29]	5	29	6.9
Agarose gel-coated tapered fiber[30]	5	55	7
RGO-coated hollow core fiber[31]	5.2	8.1	6.5
MoS_2 nanosheets based SPF[32]	0.85	0.85	13.5
MoS_2-coated etched SMF[33]	0.066	2.395	9
GO-deposited tilted fiber grating (TFG)[34]	0.042	0.115	1.5

The proposed sensor exhibits roughly equivalent response time and the fastest recovery speed within the reported groups of similar fiber-optic humidity sensors, as illustrated in Table 1. In addition, gelatin is a common, safe and inexpensive moisture-sensitive material, and the sensor is expected to be a better choice in the fields of biochemistry, food and other fields related to daily life.

A novel fiber-optic humidity sensor based on tapered micro-fiber with a deposited coating of gelatin was proposed and experimentally characterised, showing excellent performance and ultra-fast response for detecting human breath. The sensor has many advantages, including compatibility with humidity-sensing devices, simple manufacture and low loss. Gelatin is a common low-cost and high-performance, humidity-sensitive material, and its RI is closely related to ambient humidity. When the sensor is placed in different humidity environments, the variations of the effective RI of the gelatin layer have considerable impact on adjusting the loss of the MZ path, to bring a high transmission intensity difference for the sensor under different humidity conditions. The transmission intensity difference can achieve ~25 dB with a switch of breathing, which makes the sensor a highly reliable breath sensor. The ultrafast response time (84 ms) and recovery time (29 ms) and good repeatability of the sensor demonstrate the excellent capability for breath-pattern sensing. Because the materials used to construct the sensor are all safe and nontoxic, the proposed all-in-fiber humidity sensor has the great merits of low cost and environmental compatibility and could be a

promising alternative for personal health care or clinical application in the near future.

AUTHOR INFORMATION

Corresponding Author

*pengfei.wang@tudublin.ie

Notes

The authors declare no conflicts of interest.

ACKNOWLEDGMENT

This work was supported by National Key program of Natural Science Foundation of China (NSFC 61935006); The Fundamental Research Funds of the Central Universities (HEUCFG201841, GK2250260018, 3072019CF2504, 3072019CF2506); Heilongjiang Touyan Innovation Team Program; Open Fund of the State Key Laboratory on Integrated Optoelectronics (IOSKL2016KF03); 111 Project (B13015).

REFERENCES

1. Li, J.; Gai, L.; Li, H.; Hu, H., A high sensitivity temperature sensor based on packaged microfiber knot resonator. Sensors and Actuators A: Physical 2017, 263, 369-372.
2. Jung, W.-G.; Kim, S.-W.; Kim, K.-T.; Kim, E.-S.; Kang, S.-W., High-sensitivity temperature sensor using a side-polished single-mode fiber covered with the polymer planar waveguide. IEEE Photonics Technology Letters 2001, 13, 1209-1211.
3. Jiang, Y.; Fang, Z.; Du, Y.; Lewis, E.; Farrell, G.; Wang, P., Highly sensitive temperature sensor using packaged optical microfiber coupler filled with liquids. Opt. Express 2018, 26, 356-366.
4. Xing, Z.; Zheng, Y.; Yan, Z.; Feng, Y.; Xiao, Y.; Yu, J.; Guan, H.; Luo, Y.; Wang, Z.; Zhong, Y., High-sensitivity humidity sensing of microfiber coated with three-dimensional graphene network. Sensors and Actuators B: Chemical 2019, 281, 953-959.
5. Zhou, N.; Wang, P.; Shi, Z.; Gao, Y.; Yang, Y.; Wang, Y.; Xie, Y.; Cai, D.; Guo, X.; Zhang, L., Au nanorod–coupled microfiber optical humidity sensors. Opt. Express 2019, 27, 8180-8185.
6. Shin, J. C.; Yoon, M.-S.; Han, Y.-G., Relative humidity sensor based on an optical microfiber knot resonator with a polyvinyl alcohol overlay. Journal of Lightwave Technology 2016, 34, 4511-4515.
7. Troia, B.; De Leonardis, F.; Passaro, V. M., Cascaded ring resonator and Mach-Zehnder interferometer with a Sagnac loop for Vernier-effect refractive index sensing. Sensors and Actuators B: Chemical 2017, 240, 76-89.
8. Yu, H.; Xiong, L.; Chen, Z.; Li, Q.; Yi, X.; Ding, Y.; Wang, F.; Lv, H.; Ding, Y., Solution concentration and refractive index sensing based on polymer microfiber knot resonator. Applied Physics Express 2014, 7, 022501.
9. Lee, C.-L.; Liu, W.-F.; Weng, Z.-Y.; Hu, F.-C., Hybrid AG-FFPI/RLPFG for simultaneously sensing refractive index and temperature. IEEE Photonics Technology Letters 2011, 23, 1231-1233.
10. Fu, H.; Jiang, Y.; Ding, J.; Zhang, J.; Zhang, M.; Zhu, Y.; Li, H., Zinc oxide nanoparticle incorporated graphene oxide as sensing coating for interferometric optical microfiber for ammonia gas detection. Sensors and Actuators B: Chemical 2018, 254, 239-247.
11. Yan, S.-c.; Zheng, B.-c.; Chen, J.-h.; Xu, F.; Lu, Y.-q., Optical electrical current sensor utilizing a graphene-microfiber-integrated coil resonator. Applied Physics Letters 2015, 107, 053502.
12. Li, K.; Zhang, T.; Liu, G.; Zhang, N.; Zhang, M.; Wei, L., Ultrasensitive optical microfiber coupler based sensors operating near the turning point of effective group index difference. Applied Physics Letters 2016, 109, 101101.
13. Liao, Y.; Wang, J.; Wang, S.; Yang, H.; Wang, X., Simultaneous measurement of seawater temperature and salinity based on microfiber MZ interferometer with a knot resonator. Journal of Lightwave Technology 2016, 34, 5378-5384.
14. Silva, L. I.; Freitas, A. C.; Rocha-Santos, T. A.; Pereira, M.; Duarte, A. C., Breath analysis by optical fiber sensor for the determination of exhaled organic compounds with a view to diagnostics. Talanta 2011, 83, 1586-1594.
15. Mogera, U.; Sagade, A. A.; George, S. J.; Kulkarni, G. U., Ultrafast response humidity sensor using supramolecular nanofiber and its application in monitoring breath humidity and flow. Scientific reports 2014, 4, 4103.
16. Burman, D.; Ghosh, R.; Santra, S.; Guha, P. K., Highly proton conducting MoS 2/graphene oxide nanocomposite based chemoresistive humidity sensor. Rsc Advances 2016, 6, 57424-57433.
17. Jha, R. K.; Guha, P. K., Liquid exfoliated pristine WS2 nanosheets for ultrasensitive and highly stable chemiresistive humidity sensors. Nanotechnology 2016, 27, 475503.
18. Mathew, J.; Semenova, Y.; Farrell, G., Effect of coating thickness on the sensitivity of a humidity sensor based on an Agarose coated photonic crystal fiber interferometer. Opt. Express 2013, 21, 6313-6320.
19. Tan, K. M.; Tay, C. M.; Tjin, S. C.; Chan, C. C.; Rahardjo, H., High relative humidity measurements using gelatin coated long-period grating sensors. Sensors and Actuators B: Chemical 2005, 110, 335-341.
20. Wang, X.; Farrell, G.; Lewis, E.; Tian, K.; Yuan, L.; Wang, P., A humidity sensor based on a singlemode-side polished multimode–singlemode optical fiber structure coated with gelatin. Journal of Lightwave Technology 2017, 35, 4087-4094.
21. Gastón, A.; Pérez, F.; Sevilla, J., Optical fiber relative-humidity sensor with polyvinyl alcohol film. Applied optics 2004, 43, 4127-4132.
22. Peng, Y.; Zhao, Y.; Hu, X.-g.; Chen, M.-q., Humidity sensor based on unsymmetrical U-shaped twisted microfiber coupler with wide detection range. Sensors and Actuators B: Chemical 2019, 290, 406-413.
23. Shabaneh, A.; Girei, S.; Arasu, P.; Mahdi, M.; Rashid, S.; Paiman, S.; Yaacob, M., Dynamic response of tapered optical multimode fiber coated with carbon nanotubes for ethanol sensing application. Sensors 2015, 15, 10452-10464.
24. Chen, Z.; Lu, C., Humidity sensors: a review of materials and mechanisms. Sensor letters 2005, 3, 274-295.
25. Kang, B.; Heo, Y.; Tien, L.; Norton, D.; Ren, F.; Gila, B.; Pearton, S., Hydrogen and ozone gas sensing using multiple ZnO nanorods. Applied Physics A 2005, 80, 1029-1032.
26. Yi, Y.; Yu, J.; Jiang, Y.; Lewis, E.; Brambilla, G.; Wang, P., Optical interleaver based on nested multiple knot microfiber resonators. Optics letters 2019, 44, 1864-1867.
27. Darmawan, S., .; Landobasa, Y. M.; Chin, M. K., Nested ring Mach-Zehnder interferometer. Opt. Express 2007, 15, 437-48.
28. Luo, Y.; Chen, C.; Xia, K.; Peng, S.; Guan, H.; Tang, J.; Lu, H.; Yu, J.; Zhang, J.; Xiao, Y., Tungsten disulfide (WS 2) based all-fiber-optic humidity sensor. Opt. Express 2016, 24, 8956-8966.
29. Xiao, Y.; Zhang, J.; Cai, X.; Tan, S.; Yu, J.; Lu, H.; Luo, Y.; Liao, G.; Li, S.; Tang, J., Reduced graphene oxide for fiber-optic humidity sensing. Opt. Express 2014, 22, 31555-31567.
30. Bariain, C.; Matías, I. R.; Arregui, F. J.; López-Amo, M., Optical fiber humidity sensor based on a tapered fiber coated with agarose gel. Sensors and Actuators B: Chemical 2000, 69, 127-131.
31. Gao, R.; Lu, D.-f.; Cheng, J.; Jiang, Y.; Jiang, L.; Qi, Z.-m., Humidity sensor based on power leakage at resonance wavelengths of a hollow core fiber coated with reduced graphene oxide. Sensors and Actuators B: Chemical 2016, 222, 618-624.
32. Li, D.; Lu, H.; Qiu, W.; Dong, J.; Guan, H.; Zhu, W.; Yu, J.; Luo, Y.; Zhang, J.; Chen, Z., Molybdenum disulfide nanosheets deposited on polished optical fiber for humidity sensing and human breath monitoring. Opt. Express 2017, 25, 28407-28416.
33. Du, B.; Yang, D.; She, X.; Yuan, Y.; Mao, D.; Jiang, Y.; Lu, F., MoS2-based all-fiber humidity sensor for monitoring human breath with fast response and recovery. Sensors and Actuators B: Chemical 2017, 251, 180-184.

34. Jiang, B.; Bi, Z.; Hao, Z.; Yuan, Q.; Feng, D.; Zhou, K.; Zhang, L.; Gan, X.; Zhao, J., Graphene oxide-deposited tilted fiber grating for ultrafast humidity sensing and human breath monitoring. Sensors and Actuators B: Chemical 2019, 293, 336-341.

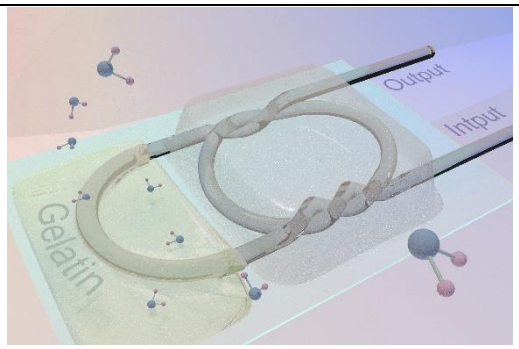

For Table of Contents only